Journal of Materials Chemistry A

Accepted Manuscript

ROYAL SOCIETY OF CHEMISTRY

www.rsc.org/materialsA

Journal of Materials Chemistry A

RSCPublishing

ARTICLE

The Effect of Energetically Coated ZrO_x on Enhanced Electrochemical Performances of $Li(Ni_{1/3}Co_{1/3}Mn_{1/3})O_2$ Cathodes Using Modified Radio Frequency (RF) Sputtering

Cite this: DOI: 10.1039/x0xx00000x

Received 00th January 2012,
Accepted 00th January 2012

DOI: 10.1039/x0xx00000x

www.rsc.org/

Ji-Hoon Lee,[a] Ji Woo Kim,[b,c] Ho-Young Kang,[a] Seul Cham Kim,[a] Sang Sub Han,[a] Kyu Hwan Oh,[a] Se-Hee Lee[*b], and Young-Chang Joo[*a,d]

To date, most coating layers for electrode materials for Li-ion batteries have been fabricated using the sol-gel method or atomic layer deposition (ALD), which involve complicated processing steps and limited candidates for coating materials. With an emphasis on solving these issues, herein, a new coating methodology based on a sputtering system was developed, and sputtered zirconium oxide was coated on $Li(Ni_{1/3}Co_{1/3}Mn_{1/3})O_2$ (L333) cathode powders. The continuous movement of the cathode powders during the coating procedure and the high kinetic energy from the sputtering process resulted in a highly uniform coating layer with multiple structures exhibiting a concentration and valence state gradient of Zr, i.e., surface (mainly Zr^{4+}) and doped (mainly Zr^{2+}) layers. The ZrO_x-coated L333 powders exhibited outstanding capacity retention (96.3 % at 200 cycle) and superior rate capability compared with the uncoated version in a coin cell with 1 M $LiPF_6$ in EC:DEC liquid electrolyte. The ZrO_x-coated L333 powders also exhibited enhanced specific capacity in a solid state battery cell with a sulfide-based inorganic solid-state electrolyte. The improved electrochemical performance of ZrO_x/L333 was attributed to the synergetic effect from the surface and doped layer: physical/chemical protection of the active material surface, enhancement of Li-ion diffusion kinetics, and stabilization of the interfaces.

Introduction

With a growing demand for large-scale and high-performance energy systems, $Li(Ni_{1/3}Co_{1/3}Mn_{1/3})O_2$ (L333) cathode material with layered structure has been intensively investigated for Li ion batteries (LIBs) for the past few decades.[1–4] L333 was developed to combine the merits and overcome the issues of one type of transition-metal-containing layered cathode, e.g., $LiNiO_2$, $LiCoO_2$, or $LiMnO_2$. The synergetic effect of Ni^{2+}, Co^{3+}, and Mn^{4+} ions constituting metal cation layers in L333 resulted in a high specific capacity of ~ 160 $mAhg^{-1}$, stabilized the layered structure, and high thermal stability.[5,6]

To achieve a high energy density, increasing the cell potential to a high limit can be considered the simplest approach. However, under these conditions, the cathode material becomes vulnerable for retaining a stable capacity because of structural and chemical instability, e.g., the dissolution of electrochemically active transition-metal cations induced by the generation of HF and undesirable reaction between the electrolyte and active materials.[7–9] In addition, the relatively lower rate capability of L333 is also one of the major drawbacks for electric vehicle applications.[10,11]

Therefore, extensive efforts have been focused on improving the structural and chemical stabilities under severe conditions. Thin

surface coating layers of metal oxides, e.g., ZrO_2, Al_2O_3, TiO_2, have been demonstrated as an effective strategy to improve the electrochemical performances of cathodes.[8,12–15] To date, most previous studies have adopted the "sol-gel"[12,16,17] and "atomic layer deposition (ALD)" methods[18,19] as the surface-coating method. The sol-gel method has some disadvantages because of the abundance of waste produced, the time-consuming nature of the process with required the use of numerous metal precursors and solvents, and post-thermal treatments to solidify the coating layer. ALD consists of a complicated cycle, i.e., precursor and reactant exposure followed by gas purging; other obstacle for this method is the insufficient available precursors to be deposited.

Sputtering, a well-established coating method in the semiconductor industry, is one of the best alternative coating methods due to its high coating efficiency, precise control of properties of the coating material, and wide range of coating materials. Despite the multi-functionality of the sputtering methodology, one challenge remains: when the conventional sputtering process is applied to powder forms of active materials, high uniformity of the coating layers is difficult to achieve because the electrode powders are irregularly exposed to the sputtered materials and they tend to form agglomerates.

Herein, a new design of a sputtering system is suggested based on the introduction of vibration motors at the same holder, which induces continuous rotation and bounce of the powder of the electrode materials. This system is effective in uniform exposure of the active material powder to the sputtered matters, thereby leading to a high uniformity of the coating layers. Even more, because of the high kinetic energy of the sputtered atoms/molecules, which can be precisely controlled, it is possible that not only the surface but also the bulk region of the active materials can be simultaneously tailored with coating species during the sputtering procedure. By careful selection of coated materials with respect to the atomic/molecular size, the structure of the active materials, including the lattice parameters and local chemical states, can be modified to enhance the electrode kinetics. In this context, zirconium oxides were selected as protective materials for a L333 cathode to demonstrate the feasibility of the modified sputtering method as a versatile coating process. ZrO_2 has exhibits a negative zeta potential, basic surface,[20] and strong bonding,[21] which are beneficial for trapping the HF and maintaining the chemical stability. Furthermore, the larger ion size of Zr than that of transition-metal cations in L333 is expected to expand the lattice parameter of the L333 cathode to facilitate the diffusion of Li ions.

The effect of an energetic coating on the electrochemical performances of L333 cathodes, e.g., the specific capacity, capacity retention, and rate capability, was investigated using two types of electrolytes: an organic liquid electrolyte (1 M $LiPF_6$ in EC:DEC) and an inorganic solid-state electrolyte (Li_2S + P_2S_5 glass). In both electrolytes, the sputtered coating layers were effective in improving the electrochemical performances based on the synergetic effect of the sputtered materials located on the surface and implanted in the bulk of the L333 powders. The mechanism for enhanced performance was elucidated based on changes in the resistance components during cycling measured from electrochemical impedance spectroscopy (EIS), the microstructural stability observed using transmission electron microscopy (TEM), and the diffusion kinetics of Li ions investigated using the galvanostatic intermittent titration technique (GITT). It was also revealed that the main factor for superior performance of coated electrodes differed depending on the electrolytes.

It is strongly believed that the modified sputtering system is a versatile coating process in that this methodology is applicable to mass production as well as serving as an advanced research tool to explore materials that could not been used in conventional coating methodologies.

Experimental

A. Preparation of ZrO_x/$Li(Ni_{1/3}Co_{1/3}Mn_{1/3})O_2$ cathodes

$Li(Ni_{1/3}Co_{1/3}Mn_{1/3})O_2$ (supplied by Johnson Controls Inc. Milwaukee, WI USA) was used as the starting material for the zirconium oxide coating. The average particle size of the NMC333 was approximately 12 μm, and each primary particle was composed of multiple grains with sizes ranging from 1 to 5 μm. The radio frequency (RF) sputtering system was modified with mechanical vibration motors held by a stainless steel beam at four edges of the holder. During the sputtering process, the vibration motors induced the continuous rotation and bounce of the powder to secure uniform exposure to the sputtered clusters. Before the sputtering of ZrO_x, the pressure of the chamber reached 1.0×10^{-6} Torr. Subsequently, a mixture gas of Ar (19 sccm, purity of 99.999 %) and O_2 (1 sccm, purity of 99.999 %) was flowed into the chamber while the base pressure was fixed at 5.0×10^{-3} Torr. The ZrO_x layer was sputtered on the L333 at room temperature and a RF power of 80 W was applied to the Zr target (purity of 99.99 %). The sputtering time was varied from 1 to 3 h.

B. Microstructural and chemical investigation

The observation of the surface morphology and analysis of the chemical element distributions were conducted using a field-emission scanning electron microscope (FE-SEM) (SUPRA 55 VP, Carl Zeiss and S4800, Hitachi). The cross-sectional samples were prepared from the cycled fully charged (200 cycles with a C-rate of 1C) uncoated and coated L333 cathodes using a dual-beam focused ion beam (FIB) (FEI, Nova Nanolab 200) and the diffraction patterns were obtained using a transmission electron microscope (TEM) (JEM-3000F, JEOL). X-ray photoelectron spectroscopy (XPS) data were collected using a PHI 5000 Versa Probe (ULVAC-PHI) and a monochromatic Al Kα X-ray source (1486.6 eV). The source power was maintained at 24.5 W.

C. Electrochemical investigation

The investigation of the electrochemical performances with an organic liquid-state electrolyte was performed using a 2032 coin-type cell using 1 M $LiPF_6$ in an EC:DEC (1:1 volume ratio) electrolyte and Li metal as the anode. The composite electrodes were prepared from the powders (uncoated and ZrO_x-coated L333), acetylene black and polyvinylidene fluoride (90:5:5 weight ratio) in N-methylpyrrolidinon. Cycling testing was conducted by using constant current followed by holding the constant voltage (4.5 V for 30 min) for the potential range of 3.0 – 4.5 V vs. Li/Li^+, and the C-rate was fixed at 1C (160 mAg^{-1}), except for the first 2 cycles (formation cycles, C-rate of C/4). For the GITT measurements, a constant current flux was supplied for 37.5 min (~ C/10) followed by a rest state for 180 min. The titration was continued within a potential range of 3.0 – 4.5 V vs. Li/Li^+.

For the electrochemical investigation of the all-solid-state cell, the glassy solid-state electrolyte was fabricated by mechanical ball milling from a mixture of 77.5 mol % Li_2S and 22.5 mol % P_2S_5 at room temperature. A schematic of the configuration of the all-solid-state cell is presented in ESI, Schematic 1†. Each layer in the cell was fabricated using the pelletizing method with a pressure between 1 – 5 metric tons. The composite electrodes were composed of the prepared powders, solid-state electrolyte, and carbon black (70:30:2) and the pelletized In_2Li alloy as the anode as well as the reference electrode. Cycling testing was conducted by constant current followed by holing the constant voltage (3.7 V for 30 min) for the potential range of 1.9 – 3.7 V vs. In_2Li, and the C-rate was fixed at C/10 (15 mAg^{-1}). All of the cycling and GITT testing were conducted using a potentiostat/galvanostat battery cycler (BT2000, Arbin)

Electrochemical impedance spectroscopy was performed using an AC impedance analyzer (1280C, Solatron analytical) in the frequency range of 20,000 – 0.001 Hz. To identify the changes in the resistance components as a function of cycle number, AC impedance spectra were obtained at the 3rd, 30th, 60th, 100th, 150th, and 200th cycles for the fully charged (4.5 V vs. Li/Li^+) cell with organic electrolytes and the 3rd, 5th, 10th, 20th, 30th, 40th, and 50th cycles for the fully charged (3.7 V vs. In_2Li) cell with inorganic solid-state electrolytes.

Results and discussion

A. The modified RF sputtering system and its effects on the coating uniformity and chemical state of L333 cathodes

Fig. 1A displays a photograph of the modified sputtering system, which was designed for coating on the powders. An innovation was performed on a substrate holder of a conventional RF sputter system. The planar holder was replaced by a ladle-shaped holder to contain the electrode powders and prohibit their loss during the sputtering procedure. Four mechanical vibration motors were attached to the edges of the ladle-shaped holder to induce continuous movement and rotation of the powders to aid uniform coating.

The uniformity of the coating layer was investigated by energy dispersive X-ray spectrometry (EDS). Fig. 1B presents the EDS mapping images with selected elements of Ni, Co, Mn, and Zr presented in the 2-h-coated cathode powders. From the image, it was confirmed that sputtered Zr was uniformly distributed on the L333 cathodes. From the X-ray diffraction (XRD) pattern for uncoated and coated L333 cathodes shown in ESI, Fig. S1†, it was revealed that sputtered zirconium oxides has an amorphous structure.

To confirm the effect of sputtering with energetic bombardment of Zr oxides on the chemical structure of the LM333 electrodes, X-ray photoelectron spectroscopy (XPS) analyses were performed. The changes in the atomic concentration of the Zr and core level spectra of Zr 3d as a function of depth are presented in Fig. 2. As observed in Fig. 2A, the variation of the atomic concentration of Zr atoms shows a concentration gradient along with the depth within the range of 100 nm investigated. Unlike the previously adopted coating methodologies, e.g., sol-gel and ALD, sputtered Zr oxides were present not only at the surface but also underneath the surface. Thus, the sputtered Zr oxides layers can be considered as the multi-layered structure composed of the surface covered layer with higher Zr concentration and Zr-doped layers formed in the bulk of L333. Fig. 2B displays the changes in the Zr 3d core level spectra along with the

depth. The red lines correspond to the peak position observed in the Zr located at the surface for the purpose of the comparison; the peak position varied with the depth. Both doublet peaks gradually shifted to negative binding energy with increasing depth. According to a previous study on the XPS analysis of Zr oxides,[22] it was confirmed that the Zr ions located at the surface have a valence state of 4+ and that the portion of the reduced form (Zr^{2+}) increased with the depth and it is speculated that the reduction of Zr^{4+} ions is a result of the ion sputtering of Ar^{+}, which is continuously flowed into the sputtering chamber during coating process.

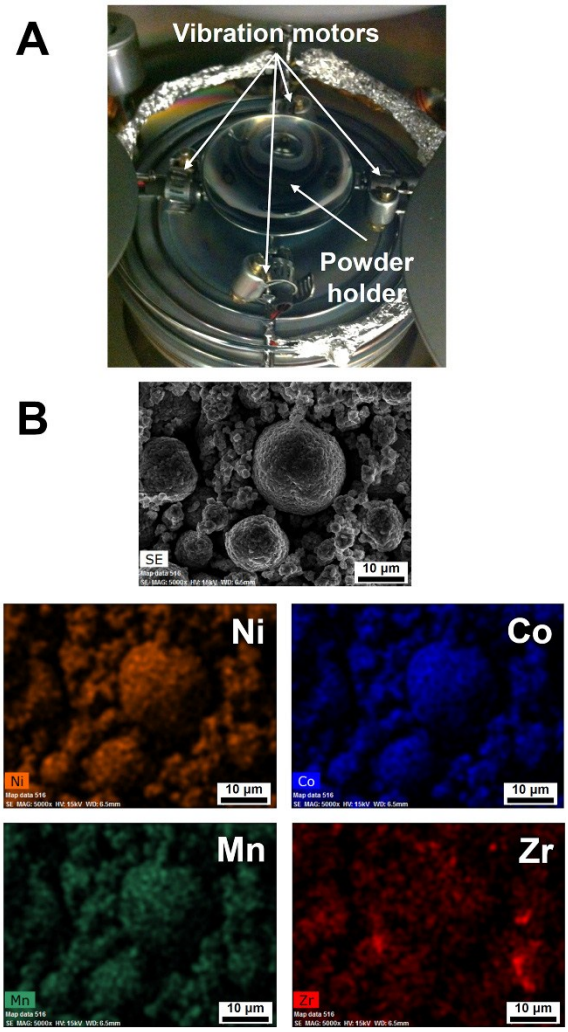

Fig. 1 (A) Photographs for modified sputtering system: four vibration motors attached to each corner of holder part to induce continuous movement of powders. (B) Energy dispersive X-ray spectrometry (EDS) mapping images of 2h-coated L333 with respect to Ni (orange), Co (blue), Mn (green), and Zr (red).

Therefore, it is assumed that the surfaces of the L333 electrodes were decorated with ZrO_2, and the reduced Zr ions, which have relatively larger ionic size than Ni^{2+}, Co^{3+}, and Mn^{4+}, were doped into the bulk, inducing the structural modification of the L333 lattice. In the following sections, the sputtered coating layer of Zr oxides will be referred to as "ZrO_x".

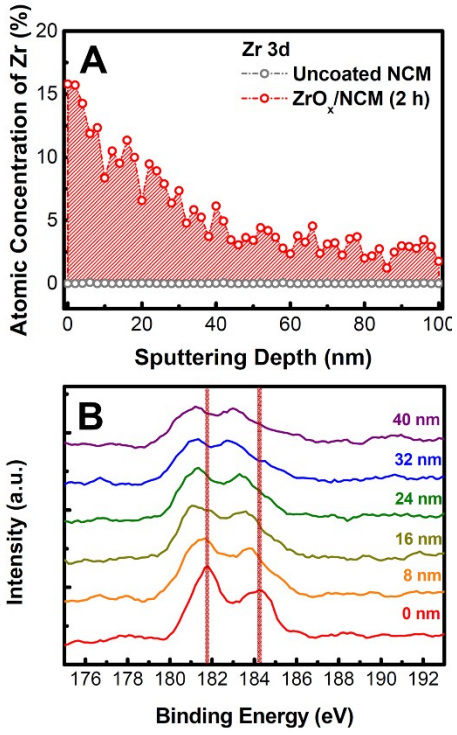

Fig. 2 (A) Changes in atomic concentration of Zr for uncoated (gray curve) and 2-h-coated (red curve) cathode powder. (B) Core level spectra of Zr 3d as a function of sputtering depth (0 to 40 nm) for 2-h-coated L333 (the two red lines indicate the peak binding energy observed at the surface (0 nm)).

B. The effect of sputtered ZrO_x layers on electrochemical performances under organic liquid electrolytes

Fig. 3A shows the cycling performance of uncoated and ZrO_x-coated (1, 2, and 3 h) L333 cathodes tested under the organic liquid electrolyte (1 M $LiPF_6$ in EC/DEC (1/v:1/v)) in the potential range of 3.0 to 4.5 V vs. Li/Li^{+}. At the 1st cycle, the uncoated L333 cell delivered a discharge capacity of 178 $mAhg^{-1}$, whereas the ZrO_x/L333 cells delivered reduced capacities with increasing sputtering time, e.g., 174, 168, and 159 $mAhg^{-1}$ for 1-, 2-, and 3-h coated electrodes, respectively. The round-trip efficiency at the 1st cycle was slightly sacrificed by introducing the ZrO_x coating layer; however, the

efficiency reached ~ 100 % for all of the uncoated and coated electrodes from the 3rd cycle.

curves of the L333 electrode reported previously.[1–4] As observed in the potential profiles of the uncoated L333 electrode (Fig. 3B), the gap

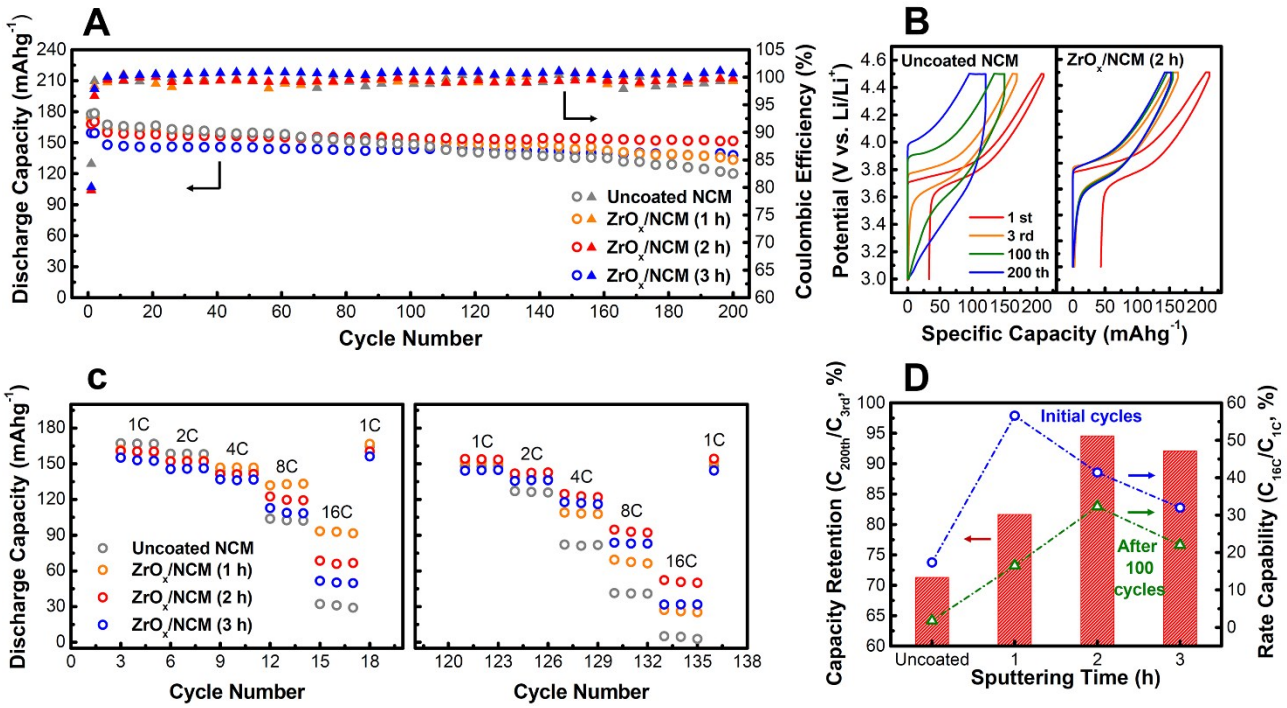

Fig. 3 (A) Discharge capacity and coulombic efficiency as a function of cycle number tested with organic liquid electrolyte (potential range: 3.0–4.5 V vs. Li/Li$^+$, C-rates: C/4 (first 2 cycles) and 1C (followed cycles)). (B) Potential profiles evolved during 200 cycles for uncoated and ZrO_x/L333 (2 h). (C) Comparison of rate capability between uncoated and ZrO_x-coated L333 initially (left) and after 100 cycles (right) (the electrodes were charged/discharged with a C-rate of 1 C for 100 cycles between two cycle regimes of rate studies). (D) Capacity retention (C_{200th}/C_{3rd}, %) and rate capability (C_{16C}/C_{1C}, %) as a function of ZrO_x sputtering time.

It is noteworthy that the cycling stability was greatly improved by ZrO_x coating. For example, the discharge capacity of the 2-h-coated L333 electrodes surpasses that of the uncoated one after 70 cycles, and the capacity retention, defined as C_{200th}/C_{3rd} (%), of the uncoated L333 electrode exhibited the lowest value of 71.3 %, whereas those for the 1-, 2-, and 3-h coated samples were 81.7, 94.6, and 92.1 %, respectively (Fig. 3D). In particular, the 2-h-coated electrodes exhibited the most outstanding capacity retention. The specific capacity (delivered at a C-rate of 1 C, 3rd cycle) as well as the capacity retention at 100 cycles of sputtered ZrO_x (2 h)/L333 electrodes (160 mAhg^{-1}/96.3 %) exhibited promising performance beyond those previously reported for surface-modified cathodes: ZrO_2/L333 coated using the sol-gel method (150 mAhg^{-1}/93.3 % [16] and 161 mAhg^{-1}/86.3 % [23]) and Al_2O_3/L333 coated using ALD (153 mAhg^{-1}/90.8 % [18]).

The potential profiles at selected cycles (1st, 3rd, 100th, and 200th) for the uncoated and ZrO_x-coated (2-h) electrodes are shown in Fig. 3B. The ZrO_x/L333 electrode shows typical charging/discharging between the charging and discharging profiles gradually widened with the cycle number. The onset potential of Li deintercalation during the charging process at the 3rd cycle is ~ 3.7 V, and the potential continuously increased and reached ~ 4.0 V at the 200th cycle, indicating that high polarization was developed during cycling. Surprisingly, the increase in polarization was greatly mitigated in the ZrO_x/L333 (2 h) electrode, and the potential profiles of the electrode were independent of the cycle number except for that at the 1st cycle (C-rate of C/4, formation cycle). As observed in the potential profiles at the 1st cycle, the coated L333 electrode exhibited a slightly larger polarization than the uncoated electrode. This larger polarization is due to the increase in both the ohmic and activation polarization caused by the ZrO_x layers. Although these contributions lead to a reduction in the discharge capacity (2.0 – 10.2 %) and coulombic efficiency (5.0 – 5.4 %) at the 1st cycle depending on sputtering time, the ZrO_x coating layer remains effective for stabilizing the active material even under a high cut-off potential of 4.5 V.

Fig. 3C presents the results of a rate study performed at 2 different ranges of cycle numbers: the initial cycles (left Fig.) and after 100 cycles with a 1C rate (right Fig.). The C-rates were determined with respect to the capacity of 160 $mAhg^{-1}$. The comparison of the potential profiles as a function of the C-rates investigated for uncoated and coated L333 electrodes are depicted in ESI, Fig. S2†. In the initial cycle regime, the specific capacity at 1st cycle (1C) was reduced with an increase in the sputtering times of ZrO_x, which agreed with the cycling performance shown in the Fig. 3A. However, as the C-rate increased, the capacity of the uncoated electrodes was rapidly decayed and exhibited the poorest capacity among all of the electrodes measured at C-rates of 8 and 16C. In this regime, the coated L333 with the thinnest ZrO_x layers (1 h) exhibited the highest rate capability, C_{16C}/C_{1C} (%) (Fig. 3D). After 100 cycles at 1C rate, for all the C-rates investigated, it was observed that the uncoated L333 delivered the smallest capacity. As shown in Fig. 3D, the rate capability of all the electrodes was somewhat decreased compared with those obtained in the initial cycle regime. However, the reduction in the rate capability was greatly relieved in relatively thick ZrO_x-coated (2- and 3-h) L333 electrodes. Therefore, the highest rate capability was achieved in the 2-h-coated L333 electrodes, which exhibit the most stable cycling retention.

C. The mechanism for enhanced electrochemical performances of ZrO_x-coated L333 cathodes.

Electrochemical impedance spectroscopy (EIS) was employed on both the uncoated and coated L333 to identify the main factor that was detrimental to the cycling performance (Figs. 4A – C). In both electrodes, the Nyquist plots showed 2 semicircles (high- and intermediate-frequency region) and sloping lines (low-frequency region). The diameters of both semicircles of the uncoated L333 (Fig. 4A) continuously increased with the cycle number, and the increasing rate of the semicircle observed in the intermediate-frequency region was much faster than that of the high-frequency semicircle. However, the Nyquist plots for ZrO_x-coated L333 did not exhibit any noticeable change, and the semicircles were much smaller. The difference in the changing tendency of the Nyquist plots along the ZrO_x layers is consistent with the changes in the potential profiles observed in Fig. 3B.

To separate each resistance contribution for the overall electrochemical reaction, an equivalent circuit model was designed, as shown in the inset of Fig. 4A. The circuit is composed of 3 resistance components (the electrolyte (R_e), surface layer ($R_{surface}$), and charge transfer (R_{ct})), 2 constant phase elements (CPE), and the Warburg impedance (W). The fitting results are denoted as solid lines in Figs. 4A and B and exhibit good agreement with the measured data. Fig. 4C shows the variation of the resistance of the uncoated and 2-h-coated L333 electrodes depending on the cycle number. Because the composition of the electrolyte and configuration of the cell were identical in all the electrodes, R_e is independent of the cycle number and exhibited the same values for both electrodes. $R_{surface}$ of the uncoated L333 increased during the early stage of the cycle and then saturated. That of the coated sample did not vary with cycling, although $R_{surface}$ measured at the 3rd cycle was slightly higher than that of uncoated L333 because of the coating layer. Based on the change of $R_{surface}$, it is assumed that the ZrO_x layer was effective in suppressing the formation of the resistive surface layer, e.g., solid electrolyte interface (SEI) layers. Accordingly, the surface resistance at the 200th cycle for the uncoated and 2-h-coated L333 was 42.9 and 28.5 Ω, respectively. The difference in the changing behavior of resistance became more apparent in the charge-transfer characteristics (R_{ct}). R_{ct} of coated L333 slightly increased during the early cycles and barely changed for the rest of the cycles, whereas that of uncoated L333 significantly increased with cycling. The relative changes of R_{ct} ($R_{ct,\ 200th}$ /$R_{ct,\ 3rd}$) for the uncoated and coated samples were 30.1 and 1.7, respectively.

When the L333 electrodes are cycled under an organic liquid electrolyte, it is believed that HF generated from the reaction of the electrolyte and trace water contents, attacks the fresh surface of L333, leading to detrimental side reactions: SEI layer formation and the dissolution of transition metal cations. For the uncoated L333, thick SEI layers forms and the dissolution of metal cations become severe because of the direct contact with the electrolyte and the product of the reactions. Therefore, the increase in $R_{surface}$ as well as high R_{ct} are observed with cycling. However, because of the basic and negatively charged surface of ZrO_2,[20] HF could be scavenged, and the direct contact between the active material and HF can be blocked by the surface-covered layers. The effect of sputtering time of the coating layer on the cycling stability is related to the capacity of HF scavenging. As the sputtering time increases, the possibilities of forming SEI layers and dissolving metal ions are reduced due to the higher capacity of HF trapping. Accordingly, all of the coated electrodes exhibited superior cycling stability compared with the uncoated one accompanied with stabilized R_{ct} and $R_{surface}$. In addition, overall, the capacity retention improves with increasing sputtering time of the ZrO_x layer.

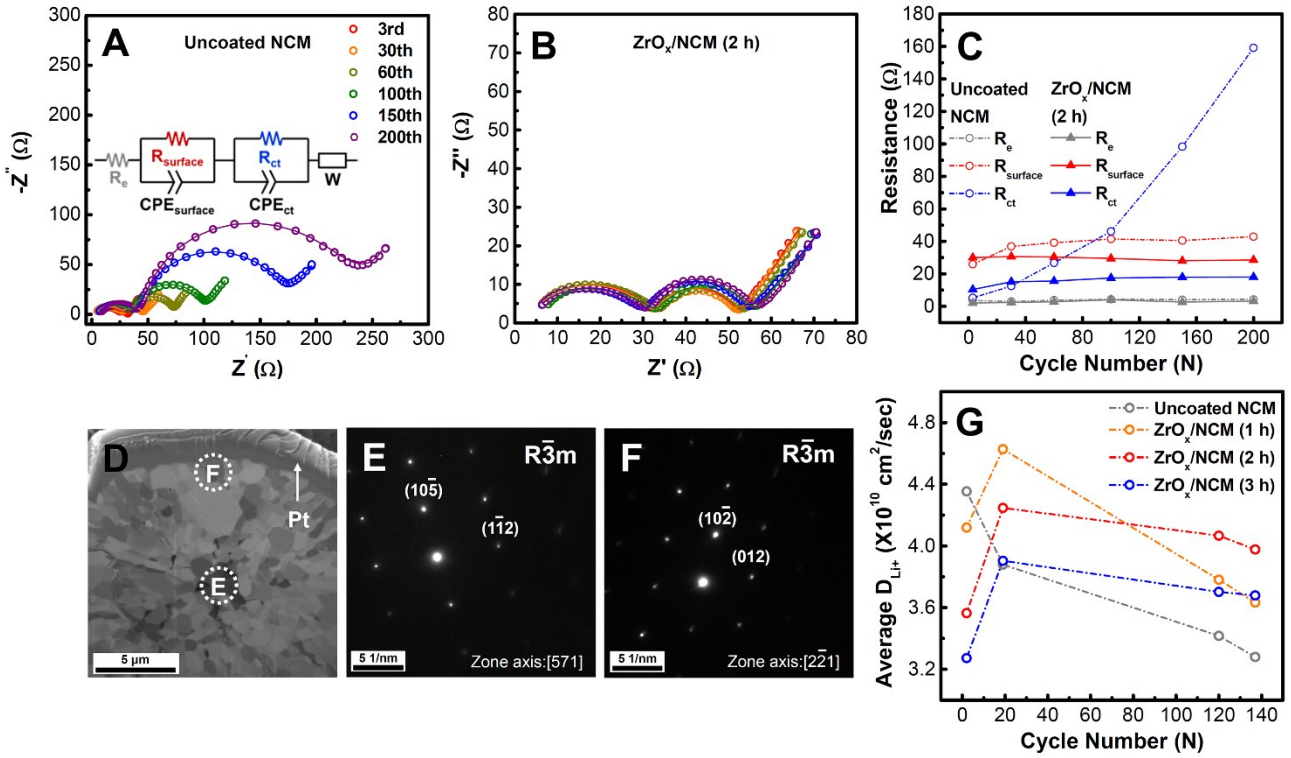

Fig. 4 Nyquist plots during cycling for uncoated L333 (A) and ZrO_x/L333 (2 h) (B) measured at fully charged state at 4.5 V (the solid lines are fitted for the measured curves using a given equivalent circuit (inset of A)). (C) Changes in resistance (R_e (electrolyte), $R_{surface}$ (surface layer), and R_{ct} (charge transfer) with cycle number calculated from fitting of Nyquist plots. (D) Focused ion beam (FIB) cross-section images of fully charged (delithiated) ZrO_x-coated (2 h) L333 powder after 200 cycles at 1C-rate between 3.0 and 4.5 V. TEM selected area electron diffraction (SAED) patterns from center (E) and surface region (F) of the particle (the specific sites where SAED patterns were obtained are denoted with dashed circles in D). (G) Change in Li ion diffusivity of uncoated and ZrO_x-coated L333 as a function of cycle number (each cycle selected for measuring the diffusivity corresponded to before and after the rate study shown in Fig. 3C).

It has been also reported that the capacity retention is sacrificed with increasing cut-off potential of the charging process for layered-structure cathodes because excessive extraction of Li leads to the irreversible phase transition to an electrochemically inactive structure.[24] According to J. W. Kim et al.,[5] the surface crystal structure of L333 undergoes a phase transition from rhombohedral structure to the spinel cubic structure with space group F3dm after 100 cycles. To confirm the effect of the ZrO_x layer on the phase transition, a single fully charged (4.5 V) ZrO_x (2 h)/L333 electrode powder was sampled using FIB (Fig. 4D) to obtain TEM selected area electron diffraction (SAED) patterns. The surface crystal structure of ZrO_x-coated L333CM preserved the original layered-structure (space group: R-3 m) even after 200 cycles, as demonstrated in Fig. 4F.

To investigate why the rate capability was improved by the introduction of the sputtered coating layer, the diffusion coefficients of Li ions (D_{Li}) of the uncoated and coated L333 were measured using the GITT at 4 selected cycles before and after the rate tests performed at 2 cycle regimes (initial and after 100 cycles). The electrodes under investigation were identical to those used for the rate study (Fig. 3C). D_{Li} was calculated using the following equation:[25]

$$D_{Li} = \frac{4}{\pi\tau}\left(\frac{m_B V_m}{M_B A}\right)^2\left(\frac{\Delta E_s}{\Delta E_\tau}\right)^2 \quad (when, \tau << \frac{L^2}{D_{Li}}) \qquad (1)$$

where τ is the holding time of the current per titration and m_B, V_m, M_B, and A are the active mass employed, molar volume of L333 (20.29 cm^3/mol [26]), molecular weight of L333 (96.46 g/mol), and contact area between the electrode and electrolyte, respectively. The parameters ΔE_s and ΔE_τ are described in ESI, Fig. S3B†.

The measured D_{Li} as a function of the electrode potential and cycle number for uncoated and ZrO_x-coated L333 electrodes are shown in ESI, Fig. S4†. Fig. 4G shows the change in the average value of D_{Li} of the uncoated and ZrO_x-coated electrodes as a function of the cycle number. The value of D_{Li} measured at ~ 3.7 V was excluded when

averaging D_{Li} because this value showed the largest deviation from that at the other potentials. D_{Li} of uncoated L333 measured before the 1st rate study (4.35×10^{-10} cm^2/sec) is comparable to the values reported in previous studies ($1.5 – 6.6 \times 10^{-10}$ (cyclic voltammetry),[2] $1.8 – 4.1 \times 10^{-10}$ (GITT),[26] and 4.4×10^{-10} (EIS)[27]). Initially, all the D_{Li} values of the ZrO_x-coated L333 electrodes were smaller than those of the uncoated one and declined as the sputtering times increased. The reduced D_{Li} observed in the coated electrodes results from the impeded Li ion diffusion through the ZrO_x layer. At the end of the 1st rate test, D_{Li} of the uncoated electrode was decreased compared with the initial value because of irreversible electrochemical processes, e.g., phase transition and formation of the SEI layer. However, the Li diffusion kinetics of the ZrO_x-coated electrodes was improved from the initial values. The increase in D_{Li} of the coated samples is assumed to be related to the transformation of ZrO_x layers into Li-ion conducting materials induced by the interaction with the reaction with Li ions in the electrolyte or initially involved in the active material during the early stage of repeated cycling. In effect, various stoichiometric Li_yZrO_z are known as materials exhibiting high Li-ion conductivity ranging from 4.9×10^{-5} to 2.4×10^{-4} S/cm.[17,28] As the transformation proceeded, the diffusion of Li ion though the coating layers was no longer restricted, and D_{Li} of the coated electrodes recovered to the original value of L333. In addition, the recovery rate of D_{Li} is inversely proportional to the sputtering time of the ZrO_x layer because thinner coating layers are more favored for fast transformation into Li-ion conducting materials, i.e., Li_xZrO_y. Therefore, the most outstanding power performance observed in the 1st rate study (Fig. 3C) was obtained in the 1-h-coated L333 electrode exhibiting the highest D_{Li}. In addition, as confirmed in Fig. 2, Zr atoms were distributed in the bulk region in reduced form. Because of the relatively larger ion size of those atoms than Ni, Co, and Mn ions, it is possible that the lattice parameters of L333 were modified or expanded upon the doping of Zr, which can facilitate the diffusion kinetics of Li ions.

During the 100 cycles after the 1st rate test, D_{Li} of uncoated as well as coated electrodes decreased but at different decreasing rates, i.e., the reduction in D_{Li} of the uncoated electrodes was more remarkable than that of the coated one. In these cycling regimes, the decrease in D_{Li} is related to the accumulation of microstructural instability, which arise from the formation of resistive layers retarding the movement of Li ions or collapse of the diffusion path of Li near the surface of active materials, accompanied with a high charging potential. Therefore, as the protecting effect of coating layers increases, the reduction in D_{Li} is relieved. The order of D_{Li} after the 2nd rate test was 2-h, 3-h, 1 h-coated, and uncoated L333, and this tendency was consistent with the rate capability (C_{16C}/C_{1C}, %): 32.3, 22.0, 16.5, and 1.8 % for 2-h, 3-h, 1 h-coated, and uncoated L333, respectively.

Therefore, the superior rate capability of coated L333 electrodes is attributed to the sputtered layer coated with high kinetic energy, which induced synergetic effects of the surface layers and doped layer inside the bulk, although only the surface layer was formed by the conventionally used coating processes. The major role of the surface and doped layers, which were introduced by the modified sputtering method with a single step, was the physical/chemical protection of active materials and enhanced Li-ion diffusion kinetics, respectively.

D. The effect of sputtered ZrO_x layers on electrochemical performances under inorganic solid electrolytes

With the strong need for new types of LIBs, e.g., large-scale batteries for EVs and printable batteries realized by 3D printers, the importance of the solid-state electrolyte (SSE) with various merits of high resistance to flammability and high flexibility to the design of the cell has been emphasized. A sulfide-based glassy material, Li_2S (77.5 mol %) + P_2S_5 (22.5 mol %), was selected as the SSE for investigating the cycling behavior of the ZrO_x-coated L333 electrodes because the this SSE is considered to exhibit high ionic conductivity based on the high polarizability as well as free volume for hopping of mobile Li defects.[29–32]

Fig. 5A shows the changes in the discharge capacity and coulombic efficiency of uncoated and ZrO_x-coated L333 cycled with solid-state electrolyte for 50 cycles. All-solid-state cells were assembled in a stainless steel framework (schematic S1) and cycled between 1.9 and 3.7 V (vs. In_2Li) with a C-rate of C/10. The In_2Li alloy was used as the counter electrode because this alloy is known to exhibit better stability against SSE than pure Li.[33] Fig. 5B shows the effect of sputtering time on the 1st discharge capacity and capacity retention (C_{50th}/C_{1st}, %). ZrO_x layers are beneficial for achieving high cycling stability, and the capacity retention is continuously increased with sputtering time: 50.2, 79.6, 83.1, and 84.7 % for the uncoated and 1-, 2-, and 3 h-coated electrodes, respectively. It is noteworthy that the ZrO_x layers also contributed to improving the discharge capacity of the entire cycles investigated and that the delivered capacity increased with sputtering time. The discharge capacities of the 1st cycle for the uncoated, 1-, 2-, and 3-h-coated L333 were 77.4, 86.4, 98.5, and 109.3 $mAhg^{-1}$, respectively. These results are opposite from those cycled under organic liquid electrolytes in that the coating layer affected the

reduction of the specific capacity of early cycles. The potential profiles (ESI, Fig. S5†) during cycling also revealed that smaller polarization was observed in the ZrO_x-coated L333 electrodes and the magnitude of polarization decreased with increasing sputtering time. whereas the increase of the resistance in the liquid-electrolyte-based cells was mainly caused by R_{ct} (Fig. 4C). $R_{surface}$ increased during early cycles and then stabilized and R_{ct} exhibited a tendency of increasing but with smaller changes than those observed in the

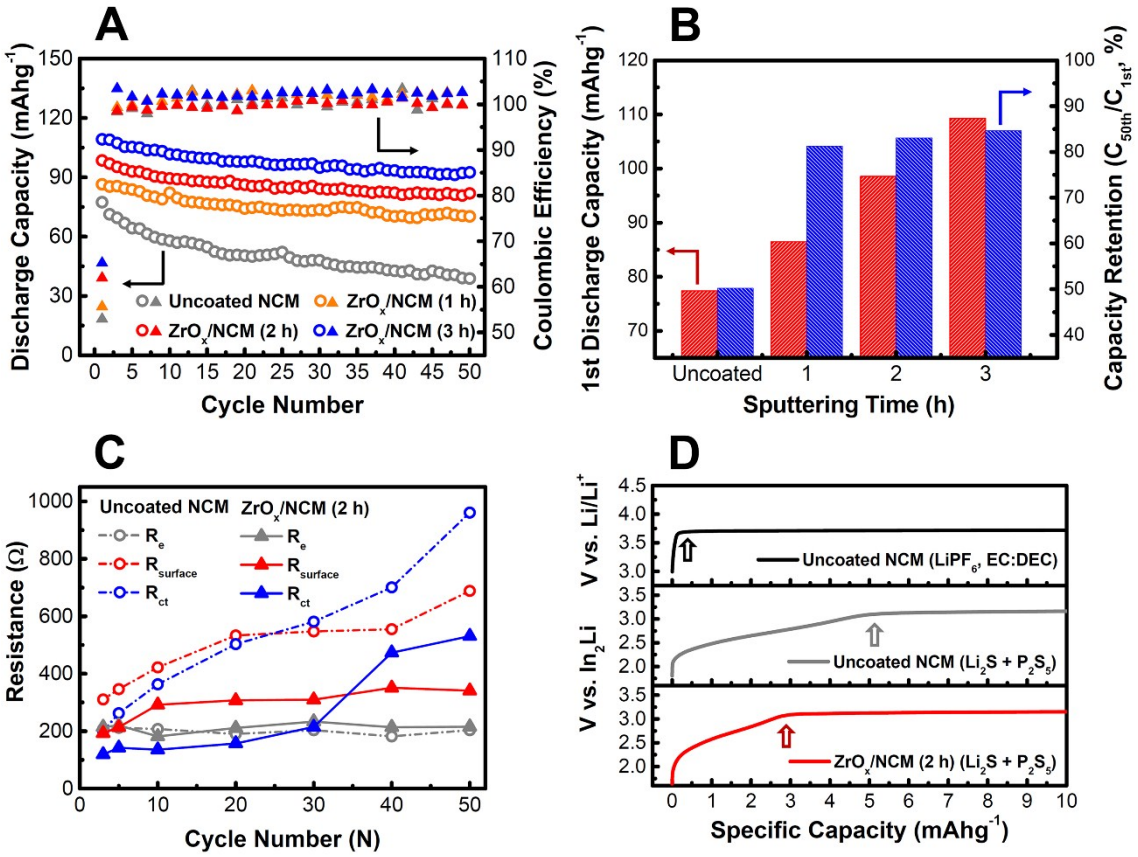

Fig. 5 (A) Discharge capacity and coulombic efficiency as a function of cycle number tested with solid-state electrolyte (potential range: 1.9 – 3.7 V vs. In_2Li, C-rate: C/10). (B) 1st discharge capacity, retention, and coulombic efficiency of 1st cycle as a function of sputtering time. (C) Changes in resistance (R_e, $R_{surface}$, and R_{ct}) with cycle number for uncoated and ZrO_x-coated L333 (2 h) measured at fully charged state (3.7 V). (D) Potential profiles during early stage of 1st charging of uncoated L333 (under liquid and solid electrolyte) and ZrO_x/L333 (2 h) (solid electrolyte).

EIS measurements were conducted on fully charged (3.7 V) uncoated and coated L333 electrodes at the 3rd, 10th, 30th, and 50th cycles, and the related Nyquist plots are presented in ESI, Fig. S6†. The changes of each resistance component (R_e, $R_{surface}$, and R_{ct}) with cycle number were calculated using the same equivalent circuit model used for simulating the liquid cells, and the results are presented in Fig. 5C. In both electrodes, R_e is independent of the cycle number but exhibited a higher value than that of the liquid electrolyte because of the retarded Li ion transport, lower conductivity than conventional liquid electrolytes,[34,35] and thicker SSE layer (~ 900 μm). In the uncoated L333 electrodes, the contribution of the surface-layer-related resistance additionally participated in increasing the total resistance, uncoated L333. The better charge transfer kinetics and surface stability obtained by the ZrO_x layer were responsible for the superior specific capacity from the beginning of cycling as well as the cycling stability.

Based on the results that the coated electrodes exhibited lower $R_{surface}$ and R_{ct} than the uncoated one even at the initial cycle and the remarkable reduction in capacity compared with that obtained in liquid cells observed in the uncoated electrodes (ESI, Fig. S7†), it can be assumed that the interfaces between SSE and L333 are detrimental for reversible Li-ion insertion/extraction.

When the interface between L333 and SSE was formed, a certain amount of Li ions was diffused into L333 to achieve equilibrium with

respect to the chemical potential of Li. Because of the electron conduction in L333, the concentration gradient of Li on the side of L333 was relieved. Therefore, the Li ions contained on the side of SSE were additionally moved to L333 to achieve another state of equilibrium. As a result, a wide Li-deficient layer was developed on the side of SSE, which is highly resistive,[34] causing high resistance (Fig. 5C) and low coulombic efficiency (Fig. 5B). As observed in Fig. 5D, a noticeable abnormal potential step (~ 3.1 vs. In_2Li) was observed for uncoated electrode during 1st charging (gray-colored line), whereas the same active material assembled with a liquid electrolyte (black-colored line) was charged without any sign of those. It can be deduced that abnormal potential steps were a result of deintercalation of Li ions, which is transferred from SSE during the equilibrium process, prior to that originally existed in the cathodes. However, the undesirable reaction involved in the potential profiles of charging was effectively mitigated by the coating layer, as demonstrated in Fig. 5D (red-colored line). The suppressed undesirable reaction reflected the higher coulombic efficiency of the 1st cycle: 52.9, 55.6, 61.9, and 65.2 % for the uncoated, 1-h, 2-h, and 3-h-coated electrodes, respectively (Fig. 5A). In the interface region of coated L333, Li ions also diffused into ZrO_x/L333 from SSE because of the differences in the concentration of Li ions between SSE and ZrO_x. However, unlike for the uncoated L333, the concentration gradient across the interface was not altered because of the electrically insulating ZrO_x. Therefore, prohibited additional diffusion of Li from SSE led to a narrower thickness of the Li-deficient region compared with the uncoated electrodes. As the width of Li-deficient region is increased, the interfaces may be acted as barriers that increase the charge transfer resistance as well as enlarge the polarization between de/lithiation reaction potentials. In fact, at the 2nd cycle, larger polarization was recognized with decrease in sputtering time (ESI, Fig. S8†).

We can suggest that an additional surface coating layer of SSEs deposited on ZrO_x/L333 as the most promising strategy to further improve the cycling stability as well as specific capacity at the level obtained in liquid-based cells.

Conclusions

A new coating methodology based on the modification of a sputtering system was developed to improve the electrochemical performances of $Li(Ni_{1/3}Co_{1/3}Mn_{1/3})O_2$ cathodes for Li-ion batteries. Highly uniform coating layers were obtained because of the continuous moving or rotation of cathode powders during the sputtering process with the aid of vibration motors. From a chemical aspect, the sputtered ZrO_x layers exhibited a concentration gradient expanding into the bulk region of the cathodes, and the valence state of Zr was changed from 4+ at the surface to 2+ in the bulk region, referring to the surface and doped layers, respectively. In a cell cycled under an organic liquid electrolyte, 1 M $LiPF_6$ in EC:DEC, all of the coated cathodes exhibited superior capacity retention and rate capability, although a slight reduction in the specific capacity during the early stage of cycle numbers also occurred. It was confirmed that the unchanged and lower polarization during 200 cycles observed in the coated cathodes was due to the suppression of the increase of the charge transfer resistance (R_{ct}), which exhibited a significant increase in the uncoated cathode. The rate capability was closely dependent on the sputtering time and cycle numbers. During the early state of cycle numbers, because of the kinetic limitation for the transformation of ZrO_x to Li-ZrO_x (Li ion conductor), the coated cathode with shorter sputtering time exhibited the highest power performance. However, as the cycle number increased, the effect of the irreversible electrochemical reaction, e.g., phase transition and cation dissolution, on the rate capability became dominant. In these cycle regimes, the coated sample exhibiting the most outstanding capacity retention provided the fastest intercalation/deintercalation of Li ions, as demonstrated by the changes in D_{Li} with cycle number. Additionally, it was revealed that the interfaces formed between the L333 cathodes and sulfide-based solid electrolytes are detrimental for reversible charge/discharge processes as well as Li storage capacity. By introducing the interposed ZrO_x layers, the interface was effectively stabilized, and the coated samples could deliver a higher capacity than the uncoated sample. The modified sputtering technique developed in this study is powerful because of its applicability to any type of coating material and because it meets the requirements of various application fields for electrochemical energy storage.

Acknowledgements

The work at the University of Colorado at Boulder was supported by the National Science Foundation (NSF, DMR-1206462).

Notes and references

[a] Department of Materials Science & Engineering, Seoul National University, Seoul 151-744, Korea.
[b] Department of Mechanical Engineering, The University of Colorado at Boulder, Boulder, CO 80300-0427, USA.

[c] Battery R&D Division, LG Chem. Ltd, Research Park, 188 Munji-ro, Yuseong-gu, Daejeon 305-738, Republic of Korea.
[d] Research Institute of Advanced Materials (RIAM), Seoul National University, Seoul 151-742, Korea.

† Electronic Supplementary Information (ESI) available: configuration of all-solid-state cell, potential profiles as a function of C-rate, result of GITT, potential profiles and EIS data for solid cells, and comparison of cycling performance of liquid-/solid-electrolyte-based cells.

1 D. D. MacNeil, Z. Lu and J. R. Dahn, *J. Electrochem. Soc.*, 2002, **149**, A1332–A1336.
2 Z.-D. Huang, X.-M. Liu, S.-W. Oh, B. Zhang, P.-C. Ma and J.-K. Kim, *J. Mater. Chem.*, 2011, **21**, 10777–10784.
3 M.-H. Lee, Y.-J. Kang, S.-T. Myung and Y.-K. Sun, *Electrochim. Acta*, 2004, **50**, 939–948.
4 B. J. Hwang, Y. W. Tsai, D. Carlier and G. Ceder, *Chem. Mater.*, 2003, **15**, 3676–3782.
5 J. W. Kim, J. J. Travis, E. Hu, K.-W. Nam, S. C. Kim, C. S. Kang, J.-H. Woo, X.-Q. Yang, S. M. George, K. H. Oh, S.-J. Cho and S.-H. Lee, *J. Power Sources*, 2014, **254**, 190–197.
6 I. Belharouak, Y.-K. Sun, J. Liu and K. Amine, *J. Power Sources*, 2003, **123**, 247–252.
7 H. Zheng, Q. Sun, G. Liu, X. Song and V. S. Battaglia, *J. Power Sources*, 2012, **207**, 134–140.
8 J. Liu and A. Manthiram, *Chem. Mater.*, 2009, **21**, 1695–1707.
9 J.-H. Park, J.-H. Cho, S.-B. Kim, W.-S. Kim, S.-Y. Lee and S.-Y. Lee, *J. Mater. Chem.*, 2012, **22**, 12574–12581.
10 H.-S. Kim, M. Kong, K. Kim, I.-J. Kim and H.-B. Gu, *J. Power Sources*, 2007, **171**, 917–921.
11 S.-H. Na, H.-S. Kim and S.-I. Moon, *Solid State Ionics*, 2005, **176**, 313–317.
12 J. Cho, Y. J. Kim, T.-J Kim and B. Park, *Angew. Chem. Int. Ed.*, 2001, **40**, 3367–3369.
13 S.-T. Myung, K. Izumi, S. Komaba, Y.-K. Sun, H. Yashiro and N. Kumagai, *Chem. Mater.*, 2005, **17**, 3695–3704.
14 Y. J. Kim, H. Kim, B. Kim, D. Ahn, J.-G. Lee, T.-J. Kim, D. Son, J. Cho, Y.-W. Kim and B. Park, *Chem. Mater.*, 2003, **15**, 1505–1511.
15 Y.-C. Lu, A. N. Mansour, N. Yabuuchi and Y. Shao.-Horn., *Chem. Mater.*, 2009, **21**, 4408–4424.
16 D. Li, Y. Kato, K. Kobayakawa, H. Noguchi and Y. Sato, *J. Power Sources*, 2006, **160**, 1342–1348.
17 Y. Huang, J. Chen, J. Ni, H. Zhou and X. Zhang, *J. Power Sources*, 2009, **188**, 538–545.
18 L. A. Riley, S. V. Atta, A. S. Cavanagh, Y. Yan, S. M. George, P. Liu, A. C. Dillon and S.-H. Lee, *J. Power Sources*, 2011, **196**, 3317–3324.
19 H.-M. Cheng, F.-M. Wang, J. P. Chu, R. Santhanam, J. Rick and S.-C. Lo, *J. Phys. Chem. C*, 2012, **116**, 7629–7637.
20 Q. Xu and M. A. Anderson, *J. Mater. Res.*, 1991, **6**, 1073–1081.
21 M.M. Thackeray, C.S. Johnson, J.-S. Kim, K.C. Lauzze, J.T. Vaughey, N. Dietz, D. Abraham, S.A. Hackney, W. Zeltner and M.A. Anderson, *Electrochem. Commun.*, 2003, **5**, 752–758.
22 G. Liu, J. A. Rodriguez, J. Hrbek and J. Dvorak, *J Phys. Chem. B*, 2001, **105**, 7762–7770.
23 S.-K. Hu, G.-H. Cheng, M-Y. Cheng, B.-J. Hwang and R. Santhanam, *J. Power Sources*, 2009, **188**, 564–569.
24 S.-C. Yin, Y.-H. Rho, I. Swainson and L. F. Nazar, *Chem. Mater.*, 2006, **18**, 1901–1910.
25 W. Weppner and R. A. Huggins, *J. Electrochem. Soc.*, 1977, **124**, 1569–1578.
26 K. M. Shaju, G. V. Subba Rao and B. V. R. Chowdari, *J. Electrochem. Soc.*, 2004, **151**, A1324–A1332.
27 X. Zhang, A. Mauger, Q. Lu, H. Groult, L. Perrigaud, F. Gendron and C.M. Julien, *Electrochim. Acta*, 2010, **55**, 6440–6449.
28 M. I. Pantyukhina, Z. S. Martem'yanova and N. N. Batalov, *Inorg. Mater.*, 2008, **10**, 1110–1114.
29 Y. Seino, T. Ota, K. Takada, A. Hayashi and M. Tatsumisago, *Energy & Environ. Sci.*, 2014, **7**, 627–631.
30 T. Ohtomo, A. Hayashi, M. Tatsumisago, Y. Tsuchida, S. Hama and K. Kawamoto, *J. Power Sources*, 2013, **233**, 231–235.
31 J. E. Trevey, Y. S. Jung and S.-H. Lee, *J. Power Sources*, 2010, **195**, 4984–4989.
32 K. Arbi, S. Mandal, J. M. Rojo and J. Sanz, *Chem. Mater.*, 2002, **14**, 1091–1097.
33 K. Takada, N. Aotani, K. Iwamoto and S. Kondo, *Solid State Ionics*, 1996, **86-88**, 877–882.
34 R. Kanno and M. Murayama, *J. Electrochem. Soc.,* 2001, **148**, A742–A746.
35 F. Mizuno, A. Hayashi, K. Tadanaga and M. Tatsumisago, *Adv. Mater.,* 2005, **17**, 918–921.

The table of contents

The Effect of Energetically Coated ZrO_x on Enhanced Electrochemical Performances of $Li(Ni_{1/3}Co_{1/3}Mn_{1/3})O_2$ Cathodes Using Modified Radio Frequency (RF) Sputtering

*Ji-Hoon Lee,[a] Ji Woo Kim,[b,c] Ho-Young Kang,[a] Seul Cham Kim,[a] Sang Sub Han,[a] Kyu Hwan Oh,[a] Se-Hee Lee[*b], and Young-Chang Joo[*a,d]*

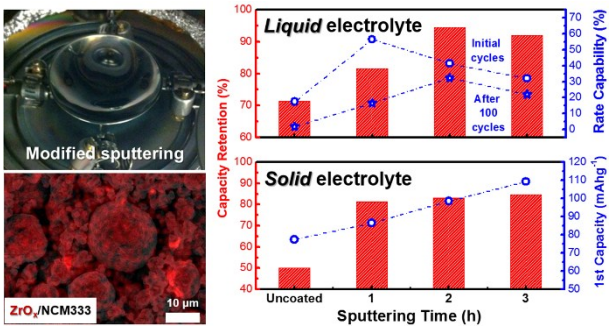

Description of TOC:

We demonstrated that ZrO_x layers on $Li(Ni_{1/3}Co_{1/3}Mn_{1/3})O_2$ cathodes deposited using novel sputtering system exhibited greatly improved electrochemical performance under both of organic liquid and inorganic solid electrolytes.

Captions of Figures

Fig. 1 (A) Photographs for modified sputtering system: four vibration motors attached to each corner of holder part to induce continuous movement of powders. (B) Energy dispersive X-ray spectrometry (EDS) mapping images of 2h-coated L333 with respect to Ni (orange), Co (blue), Mn (green), and Zr (red).

Fig. 2 (A) Changes in atomic concentration of Zr for uncoated (gray curve) and 2-h-coated (red curve) cathode powder. (B) Core level spectra of Zr 3d as a function of sputtering depth (0 to 40 nm) for 2-h-coated L333 (the two red lines indicate the peak binding energy observed at the surface (0 nm)).

Fig. 3 (A) Discharge capacity and coulombic efficiency as a function of cycle number tested with organic liquid electrolyte (potential range: 3.0–4.5 V vs. Li/Li^+, C-rates: C/4 (first 2 cycles) and 1C (followed cycles)). (B) Potential profiles evolved during 200 cycles for uncoated and ZrO_x/L333 (2 h). (C) Comparison of rate capability between uncoated and ZrO_x-coated L333 initially (left) and after 100 cycles (right) (the electrodes were charged/discharged with a C-rate of 1 C for 100 cycles between two cycle regimes of rate studies). (D) Capacity retention (C_{200th}/C_{3rd}, %) and rate capability (C_{16C}/C_{1C}, %) as a function of ZrO_x sputtering time.

Fig. 4 Nyquist plots during cycling for uncoated L333 (A) and ZrO_x/L333 (2 h) (B) measured at fully charged state at 4.5 V (the solid lines are fitted for the measured curves using a given equivalent circuit (inset of A)). (C) Changes in resistance (R_e (electrolyte), $R_{surface}$ (surface layer), and R_{ct} (charge transfer) with cycle number calculated from fitting of Nyquist plots. (D) Focused ion beam (FIB) cross-section images of fully charged (delithiated) ZrO_x-coated (2 h) L333 powder after 200 cycles at 1C-rate between 3.0 and 4.5 V. TEM selected area electron diffraction (SAED) patterns from center (E) and surface region (F) of the particle (the specific sites where SAED patterns were obtained are denoted with dashed circles in D). (G) Change in Li ion diffusivity of uncoated and ZrO_x-coated L333 as a function of cycle number (each cycle selected for measuring the diffusivity corresponded to before and after the rate study shown in Fig. 3C).

Fig. 5 (A) Discharge capacity and coulombic efficiency as a function of cycle number tested with solid-state electrolyte (potential range: 1.9 – 3.7 V vs. In_2Li, C-rate: C/10). (B) 1st discharge capacity, retention, and coulombic efficiency of 1st cycle as a function of sputtering time. (C) Changes in resistance (R_e, $R_{surface}$, and R_{ct}) with cycle number for uncoated and ZrO_x-coated L333 (2 h) measured at fully charged state (3.7 V). (D) Potential profiles during early stage of 1st charging of uncoated L333 (under liquid and solid electrolyte) and ZrO_x/L333 (2 h) (solid electrolyte).

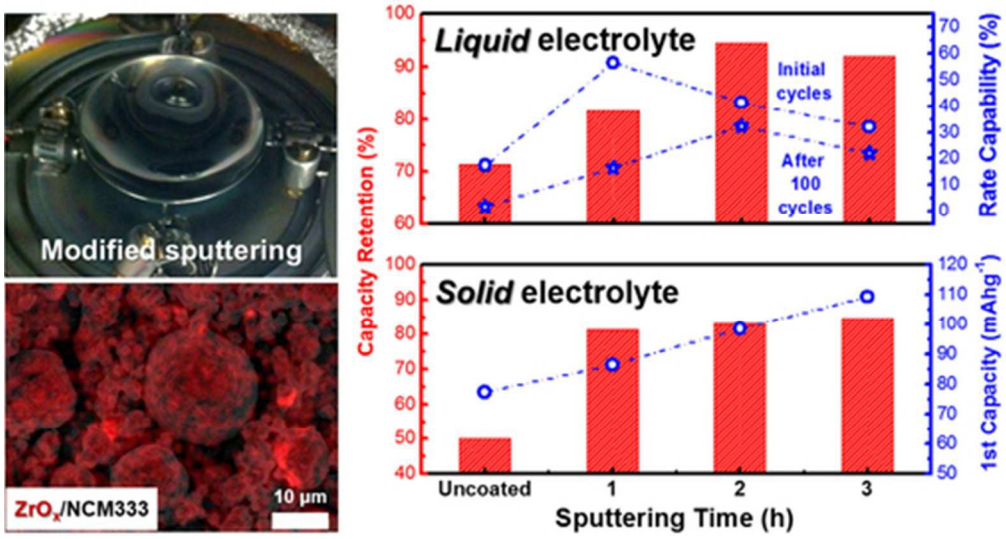

We demonstrated that ZrO_x layers on $Li(Ni_{1/3}Co_{1/3}Mn_{1/3})O_2$ cathodes deposited using novel sputtering system exhibited greatly
improved electrochemical performance under both of organic liquid and inorganic solid electrolytes.
42x22mm (300 x 300 DPI)